Instituto Superior Técnico

Computational Fluid Mechanics

HW1

Authors :

Diogo Carvalho Nº83677

José Santos Nº83704

Miguel Brito Nº83711

Gonçalo Oliveira Nº84256

Philip Widmaier Nº95467

Professors :

Prof. José Carlos Fernandes Pereira

Prof. José Manuel da Silva Chaves Ribeiro Pereira

October 24, 2019

Contents

1 Introduction

In CFD software various numerical solutions techniques are available. In this computational work we will cover the Finite Differences (FD) and the Finite Volume (FV) methods. For the FD we evaluate the first derivative of a function. For the FV we obtain the solution of the potential flow equation for a subsonic, a transonic and a supersonic case.

The first part covers the FD method. We evaluate the first derivative of the function $\phi(x) = x^2 sin(x)$. To do that we employ two different FD formulas, with different orders of accuracy and one centered while the other non-centered. First, using Matlab we calculate the approximation error in each formula. Afterwards a comparison is made between this error and the estimation of the truncation error. This is done for a range of grid sizes and presented in a single graph to be easily checked by the reader. Finally, discussion and analysis of the result is presented.

For our second part we cover the three main elements of any CFD code. We start by considering the different physical aspects of the problem. Then we explain our choice for the domain characteristics. Finally, we set the appropriate boundary conditions for each case and generate a mesh of cells. These 4 steps make up the pre-processing part of our CFD software, the first main element. For our second main element, the solver, we start by discretizing our governing equation for every small control volume (cell) in our mesh. This leaves us with a system of algebraic equations, which are to be solved by a direct or iterative and direct method. Thirdly, for our last main element, post-processing, we plot the potential, Mach and density field. We conclude the report by analyzing and commenting on some of the most pressing aspects of our results.

2 Problem 1.1: Finite Differences

For the approximation of $\frac{d\phi}{dx} (= 2x \sin x + x^2 \cos x)$, we employ a fourth-order central difference scheme (1) as well as a second-order forward difference scheme (2).

$$\left(\frac{d\phi}{dx}\right)_A = \frac{\phi(x-2h) - 8\phi(x-h) + 8\phi(x+h) - \phi(x+2h)}{12h} \tag{1}$$

$$\left(\frac{d\phi}{dx}\right)_B = \frac{-3\phi(x) + 4\phi(x+h) - \phi(x+2h)}{2h} \tag{2}$$

To determine the error of our formulas we evaluate $\frac{d\phi}{dx}\Big|_{x=2\pi}$ using Matlab and subtract its value to the one obtained by the equation (1) and (2). This is expressed in equation (3). Doing this for a range of

different grid sizes (h) we plot the result in Figure 1.

$$(Error_{analytic})_{A,B} = \left| \left(\left. \frac{d\phi}{dx} \right|_{x=2\pi} \right)_{analytic} - \left(\left. \frac{d\phi}{dx} \right|_{x=2\pi} \right)_{A,B} \right| \tag{3}$$

The Finite Differences Method is based on the Taylor Series Expansion for each considered point in the grid. However, the Taylor Series terms are only used up to the order of the derivative so the Truncation Error arises from neglecting the remaining terms of the expansions. Hence, the Truncation Error is one source of the analytic error, next to round off errors the computer makes while calculating.
By subtracting the solution of the Finite Differences Formula from the analytical expression, the Truncation Error can be obtained (eqs. 4, 5). As to perceive from the analytical expressions of the errors, the central finite difference is of 4th order of accuracy while the upwind difference is of 2nd order.

$$(Error_{truncation})_A = \frac{\phi^{(5)}(x)h^4}{30} + O(h^6) \tag{4}$$

$$(Error_{truncation})_B = \frac{\phi^{(3)}(x)h^2}{3} + O(h^3) \tag{5}$$

Plotting the truncation errors for formulas A and B also in Figure 1, it is easily observed that in general the errors decrease for smaller grid sizes h. Also, the errors decrease for higher orders of accuracy, e.g. the errors for formula A are smaller then for formula B. Since the Truncation Error dominates the analytical error, the graphs of both errors nearly superpose in certain areas for each A and B. The noise that can be seen at the graph of the analytic error of formula A (blue line in fig. 1) can be traced back to the round off errors mentioned above. For very small computational steps or rather grid sizes, the computational precision (i.e. the number of digits of a value the computer considers) is not sufficient anymore, so the values are rounded. That leads to a deviation of the actual analytical error (mainly dominated by the Truncation Error, here the green line in fig.1), so the analytical error increases.

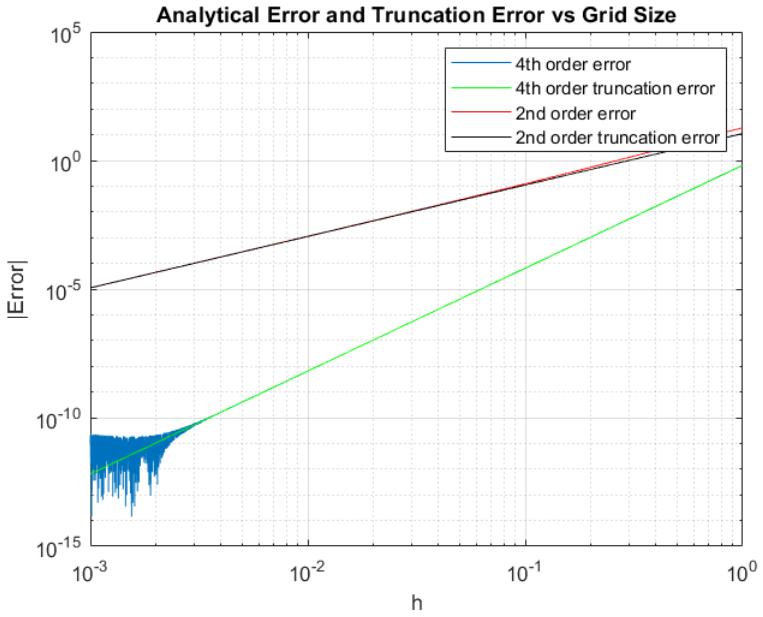

Figure 1: Analytical and Truncation Errors for formulas A and B

3 Problem 1.2: Finite Volume

3.1 Physics of the Problem

In this problem we obtain the potential field of flow over a thin airfoil, howbeit with some simplifications. The potential equation is obtained from the assumption of isentropic flow. In transonic and supersonic, shock waves are present hence, realistically, flow is not isentropic. Moreover, we apply the small perturbation theory. This renders a linear subsonic and supersonic equation (6) and a non-linear transonic equation (7).

$$\frac{\partial^2\phi}{\partial x^2}(1-M_\infty^2)+\frac{\partial^2\phi}{\partial y^2}=0 \tag{6}$$

$$\frac{\partial^2\phi}{\partial x^2}[1-M_\infty^2-(1+\gamma)\frac{M_\infty^2}{U_\infty}\frac{\partial\phi}{\partial x}]+\frac{\partial^2\phi}{\partial y^2}=0 \tag{7}$$

The strategy to tackle the non-linearity is through an iterative solver explained in section solvers. In our simulation, the Mach numbers of the undisturbed flow for each case are presented in table1. This flow only has a horizontal component of the velocity, U_∞. Taking as reference values of temperature $T=288K$, specific gas constant for air $R=287JKg^{-1}K^{-1}$ and heat capacity ratio $\gamma=1.4$ and using the expression $U_\infty=M_\infty\sqrt{\gamma TR}$ we get the values for U_∞ in table 1. The airfoil simulated is a two-dimensional diamond shaped one with values of chord $c=1m$ and thickness $t=0.06c=0.06m$. Due to the fact that the potential field flow of the problem is symmetric with respect to the chord of the airfoil (x axis) this simulation is only processed for the upper half of it. We know the inviscid flow must obey the boundary

condition that dictates fluid has to be tangent to the surface. There is no fluid going in or out of the impermeable interface. For the condition previously stated to be respected: $\frac{v}{u+U_\infty} = \frac{dy}{dx}$, where y is the shape of the airfoil. Because $U_\infty >> u$ and by the definition of potential we get: $\frac{\partial \phi}{\partial y} = v = \frac{dy}{dx} U_\infty$. Finally, substituting with numerical values, where $\frac{dy}{dx} = tan\theta = \frac{t/2}{c/2} = \frac{t}{c} = 0.06$, we get the last row in table 1.

	Subsonic	Transonic	Supersonic
M_∞	0.5	0.9	1.6
$U_\infty(m/s)$	170.09	306.16	544.28
$\frac{\partial \phi}{\partial y} = \frac{dy}{dx} U_\infty(m/s)$	10.21	18.37	32.66

Table 1: Physical values of the problem

3.2 Domain Characteristics

The fluid, realistically, is undisturbed only very far away from the airfoil (source of perturbation). Recreating the same conditions however would mean choosing dimensions of the grid which make the solution of the problem unbearable from a computational point of view. This would also mean sacrificing precision and accuracy in calculating the equation near our area of most interest, i.e., the airfoil. In order to deal with this unavoidable setback, we must choose a grid size which assumptions about unperturbed flow at the boundaries do not induce too large of an error in the calculations. In this simulation the grid has a size of 5m (horizontally) by 5m (vertically) for all flows. Nevertheless, the position of the airfoil changes between all 3 situations. The Airfoil in the subsonic flow makes the most sense to be in the middle, since the perturbations propagate both upstream and downstream. It is also interesting to note the mirroring of the potential about the value x in the middle of the airfoil. For the transonic situation because of the presence of subsonic flow it still is best to center the airfoil in the grid. Finally, in the supersonic case, owning it to its physical proscriptions there is no special care to be taken about the distance between the airfoil and the left boundary of the grid. Whereas in the 2 previous potential flow perturbations propagate upstream, supersonic perturbation reach is limited by a left-running wave (for the upper portion of the airfoil and right-running waves for the lower portion). The wave angle can be easily calculated and that will be done further down this report in order to compare it to the angle obtained in the simulation. The left-running wave only goes downstream of the source of perturbation. The assumption of an undisturbed flow upstream of the body is not an approximation anymore regardless of its distance to the airfoil. In conclusion, we decided to place the airfoil closer to the left boundary.

3.3 Boundary Conditions

For the subsonic flow, we impose a zero Dirichlet boundary condition to the left and right of the domain. Graphically this means equipotential lines are parallel to the grid line. The upper boundary is a zero

Neumann condition ($\frac{\partial \phi}{\partial x} = 0$), ie, there is no variation of the potential in the y direction. Graphically this means equipotential lines leave the grid at a 90 degree angle. Finally, in the lower section of the grid we have 3 boundary conditions. Both Neumann, albeit, one null and the other 2 non-zero constants. Firstly, outside of the values of x where the airfoil is represented we have $\frac{\partial \phi}{\partial x} = 0$. In the region where the airfoil is to be placed, as mentioned in the first section (physics of the problem), the flow over the airfoil must respect the condition $\frac{\partial \phi}{\partial y} = U_\infty \frac{dy}{dx}$. It should be noted that $\frac{dy}{dx}$ is positive for the first half of the profile and negative for the other half. For the supersonic flow, the boundary conditions of the upper and lower sides of the grid are the same as the subsonic ones. For supersonic however, because we use regressive derivatives in the x direction which use the 2 points behind we impose the 2 boundary conditions on the left side instead of one on each side. Beyond the zero Dirichlet condition used in the previous case, we also impose a zero Neumann condition in order to cope with the lack of regressive points needed to obtain the flux in the boundary cells. This approximation is justified if we suppose the existence of 2 extra points (ghost points) outside our domain. The value of the potential of both points has to be zero ($\phi = 0$) because they are to the left of our boundary where ϕ is also assumed null. Finally, for the transonic case the upper and lower B.C. are the same. The left and right conditions depend on the M_∞ used. Because we used a $M_\infty < 1$ boundary conditions for upstream and downstream limits of the domain are duplicated from the Subsonic case.

3.4 Mesh

There is an endless list of mesh options. Different problems require different grids, so this choice is of paramount importance in any CFD simulation. A structured grid is, in general, the most "natural" for flow problems as the grid lines follow in some sense the streamlines. It should be stated moreover that in comparison with unstructured grids, structured ones are more efficient in terms of accuracy, CPU time and memory requirement. That being said, we can assert that the use of unstructured grids is only justified when working with complex geometries. Due to the lack of any geometry complexity in our simulation, it is apparent the employment of a structured grid. In addition to being structured, a uniform Cartesian grid, where all the points are equidistant and all the cells are perfect cubes, was implemented. This is the ideal mesh by virtue of having the highest possible accuracy of the discretized formulas. Working in the absence of solid walls this made the most sense. To recap, we adopted a structured uniform Cartesian grid with 150 number of cells in the x-direction and 150 cells in the y-direction. Considering the domain dimensions we promptly check equal width and height values for each cell, these being $dx = dy = \frac{5}{150} = 0.03(3)$.

3.5 Numerical Schemes

In the finite volume method we start by discretizing our governing equation for every cell. In order to be able to do this we must introduce some numerical approximations. First, we integrate the governing equation over the control volume. Secondly, applying the Gauss Theorem we convert the volume integrals

in fluxes over the cell faces. These steps are represented in equation (8).

$$C\frac{\partial^2\phi}{\partial x^2}+\frac{\partial^2\phi}{\partial y^2}=0\Rightarrow C\int\frac{\partial^2\phi}{\partial x^2}dV+\int\frac{\partial^2\phi}{\partial y^2}dV=0\Rightarrow C\int\frac{\partial\phi}{\partial x}\cdot\vec{n}dS+\int\frac{\partial\phi}{\partial y}\cdot\vec{n}dS=0 \tag{8}$$

It is now that we introduce the first numerical approximation in our calculation, which is assuming the average value over the face as its value at the center point. This leaves us with equation (9). This equation is in a generic form, meaning that it is applied in every cell of the mesh.

$$-C\left.\frac{\partial\phi}{\partial x}\right|_w S_W+C\left.\frac{\partial\phi}{\partial x}\right|_e S_E-\left.\frac{\partial\phi}{\partial y}\right|_s S_S+\left.\frac{\partial\phi}{\partial y}\right|_n S_N=0 \tag{9}$$

In FV, variables are known only in the middle of the cell. In order to obtain the value at the face we have to interpolate, our second approximation. The potential does not have steep variations so a linear interpolation (2 points) was deemed sufficient. This scheme is second-order for uniform grid, such as ours. For $M<1$ information reaches both up- and downstream. For this reason, we use one point on the right and another on the left of the cell face. When $M>1$ information only comes from upstream. To respect this physical constraint our interpolation uses both cells to the left of our cell face. This translates into, using the West face as an example, the subsonic and supersonic flux being calculated as presented by equations (10) and (11), respectively.

$$\left.\frac{\partial\phi}{\partial x}\right|_w S_W=\frac{\phi_P-\phi_W}{\triangle x}\triangle y=\phi_P-\phi_W \tag{10}$$

$$\left.\frac{\partial\phi}{\partial x}\right|_w S_W=\frac{\phi_W-\phi_{WW}}{\triangle x}\triangle y=\phi_W-\phi_{WW} \tag{11}$$

After applying this process to every cell, with the appropriate boundary conditions, we can represent the coefficients of a horizontal grid line as a single matrix, our B matrix. It should be noted that transonic matrix is a mixture of the supersonic and subsonic rows depending on whether $C<0$ or $C>0$, accordingly.

$$B_{subsonic}=\begin{bmatrix}-(3C+1) & C & & & & & \\ C & -(2C+1) & C & & & & \\ & & \ddots & & & & \\ & & & C & -(2C+1) & C & \\ & & & & -(3C+1) & C & \end{bmatrix}^{(N\times N)}$$

$$B_{transonic} = \begin{bmatrix} -(3C+1) & C & & & \\ C & -(2C+1) & C & & \\ C & -2C & C-1 & & \\ & & \ddots & & \\ & & & -(3C+1) & C \end{bmatrix}^{(N\times N)}$$

$$B_{supersonic} = \begin{bmatrix} (2C-1) & & & & \\ -3C & (C-1) & & & \\ C & -2C & C-1 & & \\ & & \ddots & & \\ & & C & -2C & C-1 \end{bmatrix}^{(N\times N)}$$

Finally combining all the lines we get matrix A, which represents the coefficients for the whole grid.

$$A = \begin{bmatrix} B & I & & & & & \\ I & B-I & I & & & & \\ & & \ddots & & & & \\ & & & I & B-I & I & \\ & & & & I & B & \end{bmatrix}^{(N^2\times N^2)}$$

3.6 Solvers

Solvers, in CFD, refer to the method used to solve our system of linear equations. Working with matrices we have a couple of different choices. We can either use an iterative or a direct method to invert our matrix. In this case, to solve equation (12).

$$A\phi = B \Longleftrightarrow \phi = A^{-1}B \tag{12}$$

In this simulation, our mesh and subsequently our matrix A is relatively small, in a computational point of view. For this reason we prioritized a Matlab direct method over an iterative one. As already mentioned, the transonic equation is non-linear. In the previous section we assume the $\frac{\partial^2\phi}{\partial x^2}$ coefficient (C) as a constant, even though, it depends on our solution, ϕ. To do this we start with an initial value for our potential. We chose a subsonic solution. This allows us to obtain the value of C for the first iteration. We proceed in a similar fashion to the subsonic and supersonic case, using a Matlab direct solver to solve equation (12). Applying an under-relaxation factor (URF=0.1) we get a new solution for the potential, meaning $\phi^{n+1} = 0.1\phi_{new} + 0.9\phi_{old}$. We can use this new potential solution to obtain the value of C and

start this process all over again, iterating until the residuals converge. The convergence threshold is shown in equation (13). The residuals decay is plotted in Figure (2).

$$\epsilon = A(\phi^n)\phi^n - B < 10^{-4} \tag{13}$$

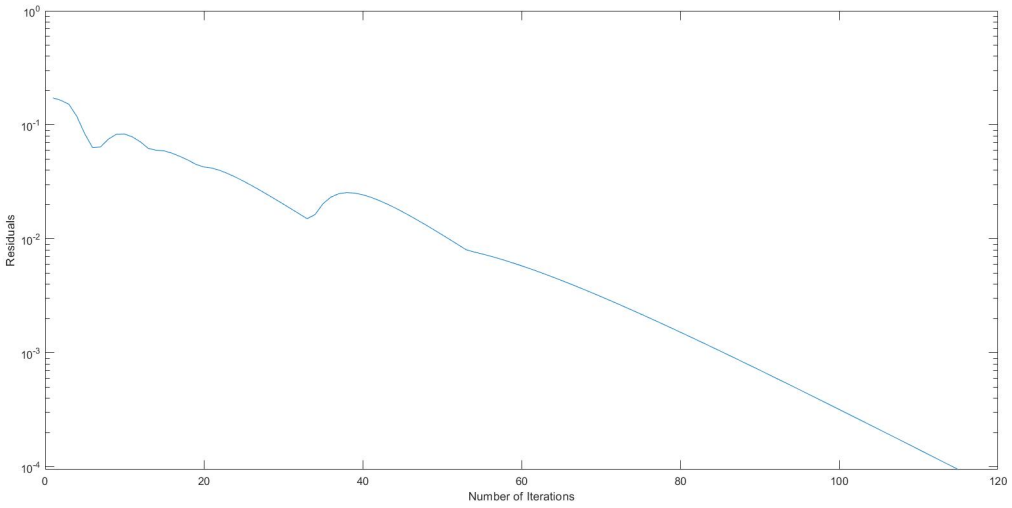

Figure 2: Error decay over iteration number

Iterations	Solver	dim(A)	Tolerance	MaxSolverIter	max(error)	Time(s)
75	*qmr*	22500^2	1×10^{-6}	1000	0.01681	141.3
75	*qmr*	22500^2	1×10^{-6}	2000	0.01681	141.4
75	*qmr*	22500^2	1×10^{-8}	200	0.1351	106.3
75	*qmr*	22500^2	1×10^{-8}	20000	0.01681	152.5
75	*qmr*	22500^2	1×10^{-6}	1000	0.01681	141.3
150	*qmr*	22500^2	1×10^{-8}	200	0.1258	215.0
150	*qmr*	22500^2	1×10^{-8}	20000	0.00111	305.8
75	$A\backslash B$	22500^2	–	–	0.01681	107.8
150	$A\backslash B$	22500^2	–	–	0.00111	214.5

Table 2: Solver parameters and results

3.7 Subsonic Results

For the subsonic regime a mach number $M = 0.5$ was considered. In the area where the airfoil would be placed, because of how it was defined, results are merely mathematical and hold no real physical meaning. It can also be observed that with the airfoil centered, field lines are symmetrical over the mid chord line. Looking at the potential and mach figures (3 and 4), there is a deceleration as the flow approaches the

the leading edge of the airfoil, represented by the darkening of the lines. It then accelerates up until the vertice, where speed is maximum, and decelerates again, conferring the symmetry previously mentioned. As for the density field, figure (5), it has no significant variation outside the vertice region. Lastly, it is also worth noticing that far from the airfoil, potential is null. In this region speed is constant and it means the airfoil exerts no influence over the flow.

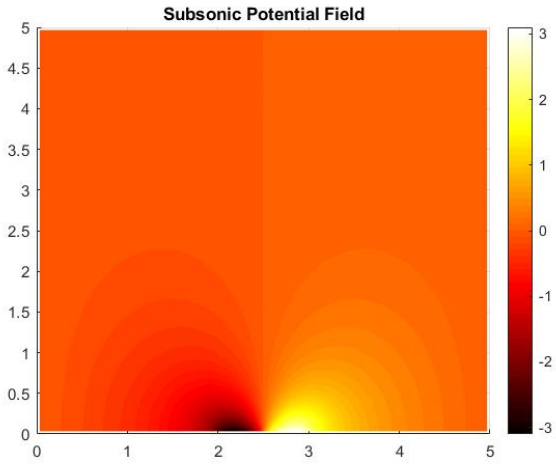

Figure 3: Subsonic Potential Field

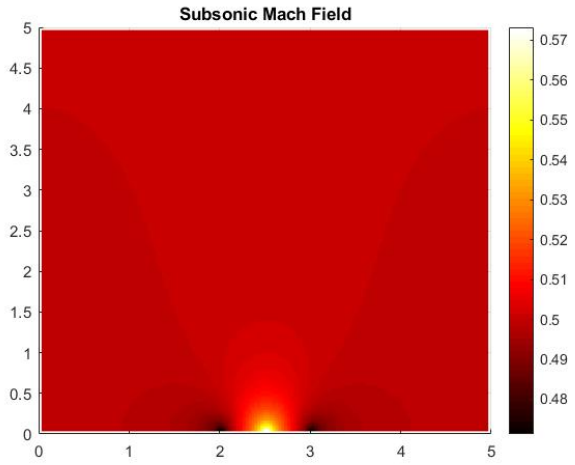

Figure 4: Subsonic Mach Field

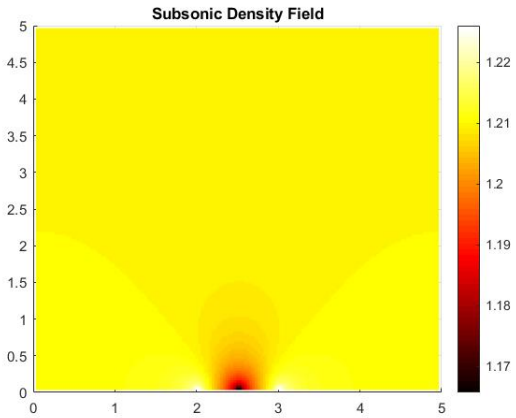

Figure 5: Subsonic Density Field

3.8 Supersonic Results

In this case, potential gradients are much larger than in the subsonic case, reflecting the larger changes in speed. It can be seen that upstream the airfoil, the potential is null, so in this region, the flow has infinity conditions. After the leading edge the potential decreases until the mid chord and then gets restituted in the second half, returning to zero after the trailing edge. Or, in terms of speed, there is a deceleration at the leading edge and a local acceleration at the vertice, as can be observed in figure (7). The analytical

result for the angle of oblique shock obtained through the $\beta - \theta - M$ relation, expressed on equation (14), was 46.44º.

$$\tan\theta = 2\cot\beta \frac{M_1^2 \sin^2\beta - 1}{M_1^2(\gamma + \cos 2\beta) + 2} \tag{14}$$

There is a disparity between analytical and computed results due to the fact that the analytical result takes into account θ and mach whereas the computed one only depends on mach. In the table below are presented the computed results for different grid sizes, which shows that the error increases with the number of cells.

Cell nr	**70x70**	**150x150**	**200x200**	**300x300**
β	45.72º	42.71º	42.15º	40.81º

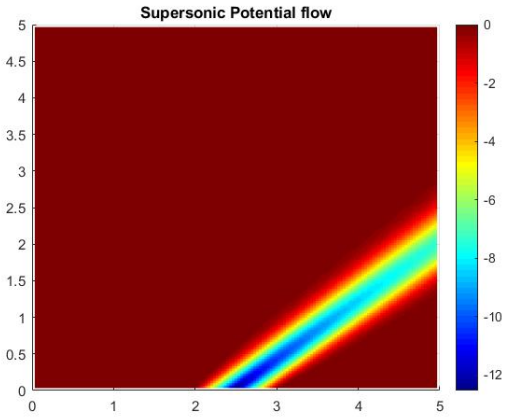

Figure 6: Supersonic Potential Field

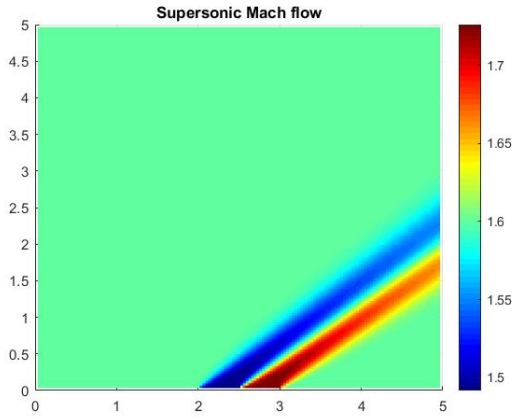

Figure 7: Supersonic Mach Field

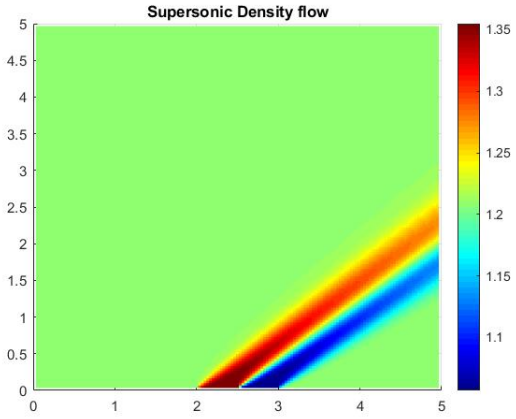

Figure 8: Supersonic Density Field

3.9 Transonic Results

Lastly, transonic results will be discussed. As mentioned previously in section *Solvers*, our initial solution will be subsonic for M=0,8, this value was chosen to have a more accurate potential before starting to iterate towards our final solution with M=0,9. Transonic flow has characteristics of both the subsonic and supersonic results, which were already discussed in this report. Most of the domain will be dominated by subsonic flow, therefore the potential field will be heavily influenced by the airfoil, which is located in the middle of the X domain. However, supersonic flow will also occur on the middle of the airfoil when the flow is accelerated.

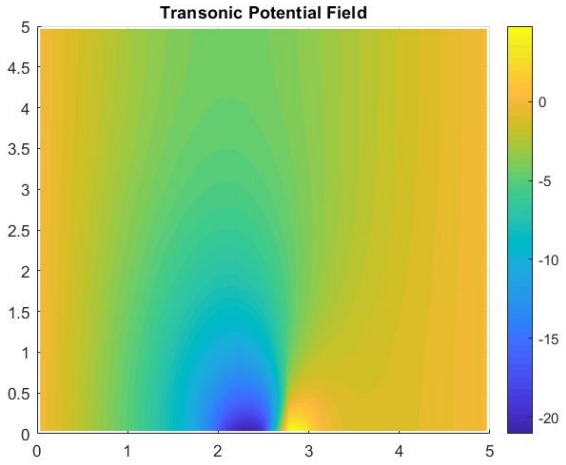

Figure 9: TransonicPotential field

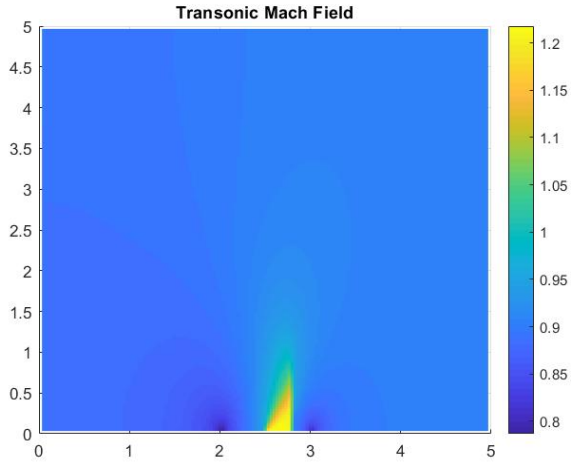

Figure 10: TransonicMach field

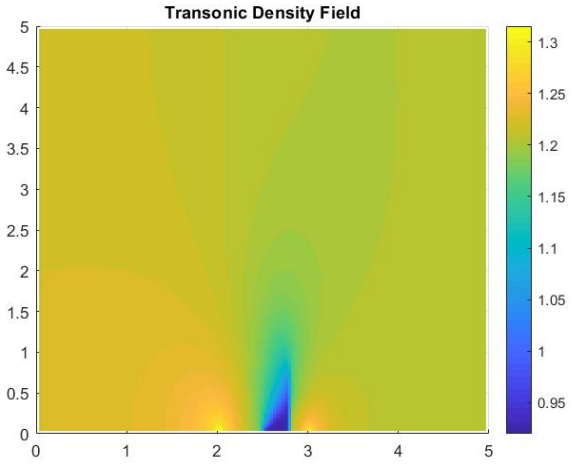

Figure 11: Transonic Density field